40th Fluid Dynamics Conference and Exhibit
28 June - 1 July 2010, Chicago, Illinois

AIAA 2010-4620

A Model of Lateral Line of Fish for Vortex Sensing

Zheng Ren[Ł] and Kamran Mohseni[y]
Department of Aerospace Engineering Sciences, University of Colorado, Boulder, CO 80309-429

Abstract

In this paper, potentail flow theory is adopted to model the flow field around a fish-like body. A two-dimensional inviscide model has been developed, and pressure distribution on the body surface has been computed according to the model. The lateral line trunk canal (LLTC) of a fish is modeled. With the external flow known, the flow inside LLTC driven by the pressure gradient between a pair of consecutive pores has been solved analytically. Furthermore, parametric studies are performed in order to determine the e ect of various flow parameters on the pressure distribution on body surface and flow inside LLTC. The cases of fish-like body in free stream alone, with single vortex close to one side of the body and a vortex street passing by the body are studied. The results show that the signature of the vortex street can be detected by measurement of the flow velocity changing with time inside LLTC. It is reasonable to suggest that the LLTC of a fish is able to detect the signature of the wake vortices shed by an object near by. The resolution of the LLTC sensing a certain vortex street is also discussed base on the the model.

Nomenclature

c	chord length of the fish-like body
l	horizontal distance between vortices
b	vertical distance between vortices
h	vertical distance between fish and vortex street
	complex coordinates before Joukowski Transformation
z	complex coordinates after Joukowski Transformation
a	radius of the cylinder
	velocity potential
u_c	flow velocity inside the canal
	circulation strength of vortex
Ð L	distance between adjacent pores in lateral line
$!^{Ł}_{D}$	kinetic Reynolds number
U_1	free stream velocity at infinity
U_{tr}	velocity of vortex street in static fluid
U_s	velocity of vortex street
C_p	pressure Coe cient

1 Introduction

All fishes possess a mechanosensory lateral line system, which responds to the surrounding water motion relative to the fish's skin. This sensing system consists of superficial neuromast (SN) and canal neuromast (CN) subsystems. SNs are located on the skin surface of a fish, extending into external fluid, while CNs are buried inside the lateral line which. The basic sensing unit of the two neuromast is hair cell of fish.

[Ł] Graduate Student, Department of Mechanical Engineering.
[y] Associate Professor, Department of Aerospace Engineering, Associate Fellow of AIAA.

Such hair cell will deflect under oncoming flow, and thus the flow can be detected by hair cell. SNs are generally smaller in diameter than CNs and contain fewer hair cells compared with CNs [1]. The lateral line organ is capable of diverse sensing tasks from the detection of near field motion [2] produced by prey [3], predator [4] or during schooling [5], to the perception of static obstacles [6]. Previous research has shown that superficial neuromasts respond to changes in external flow velocity, while canal neuromasts respond to changes in external flow acceleration (associated with corresponding changes in external flow pressure) around the fish [7]. An easy suggestion would be that CNs sense the information of pressure gradient created by stimulus in distance while SNs are more for velocity of the surrounding flow.

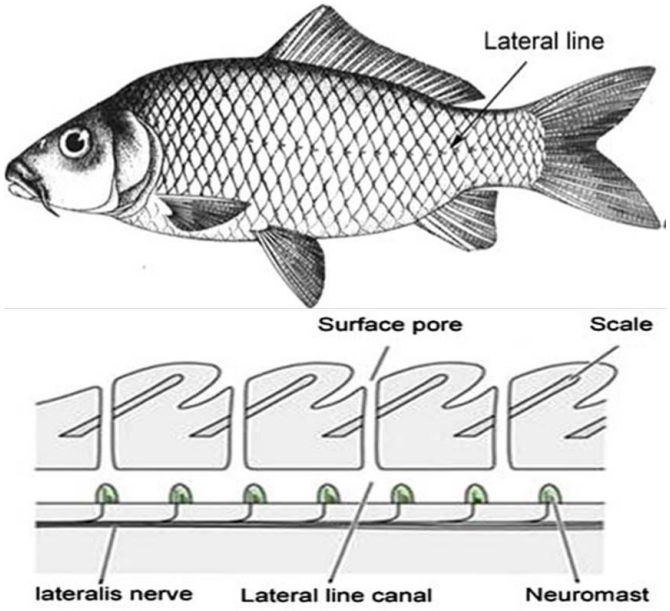

Figure 1: Schematic of lateral line of a fish and the neuromast in a canal from van Netten [8]

Models using potential flow theory have been proposed in the past to find the pressure distribution on the fish skin in the presence of stimulus. In potential flow theory, the viscosity of fluid is neglected, thus the boundary condition at a solid body requies only that the velocity normal to the wall is equal to the wall velocity. The potential dipole source flow equations were used to model the vibrating sphere near a fish body [9]. The same equation was used by Kroese to compute the slip velocity along the fish skin caused by a nearby vibrating sphere [10]. Potential flow around a three-dimensional slender body with a circular cross-section has been obtained by Handelsman and Keller [11]. Hassan adopted this solution to investigate the case of fish moving in open water and of gliding towards a plane surface [12], gliding alongside or above a plane surface [13] and oscillating sphere near the fish [14].

Numerical modeling of external flow due to the presence of a vortex street shed by a prism was studied in two dimensions, and internal flow modeled in three dimensions with hair cells was then computed [15]. However, the flow inside the LLTC has never been considered over the entire length of the canal. Because of openings along the canal, internal flow velocity is not expected to be uniform, which suggests the distribution of velocity along the LLTC may contain rich information on external flow. The purpose of this study is to investigate the information captured by the LLTC with presence of a vortex street in external flow. Potential flow theory is used to model the external flow field in two dimensions, and pressure distribution along the fish skin is calculated accordingly. The internal flow is also modeled analytically to calculate the velocity distribution along the LLTC.

2 Theoretical Modeling

The flow field created by swimming fishes or obstacles in streem can be detected by the Lateral Line of a fish. The information of such object is revealed in the wake generated by the object, which is generally in the form of a Karman vortex street. In this study, the flow field of a vortex street passing by a fish-like body is investigated. Potential flow theory has been used to model the external flow field. In this section, a two-dimensional potential flow model is presented to determine the pressure field around a fish-like body, following which an analytical model characterizing flow inside the LLTC is presented.

2.1 External flow field modeling

In order to use potential flow theory, the external flow field is assumed to be inviscid and irrotational, and only considered in two-dimensions. The profile curve of a fish body can be obtained by using Joukowski Transformation [16]. The flow over a cylinder with radius a can be mapped into the flow around a fish-like body as given by:

$$z = \quad + \frac{c_0^2}{\quad}: \tag{1}$$

The cord length c of the body is determined by

$$c = 2c_0 \quad [(c_0 \quad 2a) + c_0^2=(c_0 \quad 2a)] \tag{2}$$

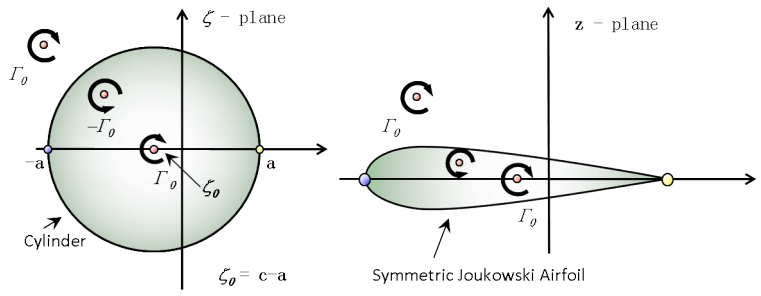

(a) coordinate frame (b) z coordinate frame

Figure 2: Flow field before and after Joukowski Transformation.

The presence of a vortex street is achieved by proper placing of 2D point vortices on one side of the body. The locations of those point vortices are first determined in z plane, then their corresponding locations in plane are calculated according to Inverse Joukowski Transformation. Solving for the inverse Joukowski Transformation (z to coordinate mapping) of Equation (1) for results in a multi-valued solution:

$$= \frac{1}{2} \quad z \; \check{s} \quad \sqrt{z^2 \quad 4c_0^2} \quad : \tag{3}$$

The implications of this function is that there are two possible coordinates in the cylinder frame for each z coordinate in the plate frame. One of the coordinates is outside of the cylinder and the other is inside of the cylinder. Therefore, in order to properly map a z coordinate to the appropriate coordinate, the following condition is applied to ensure it is outside the bounds of the cylinder: The corresponding coordinate to a respective z coordinate will be the solution in Equation (3) where the magnitude of the point is greater that the radius of the cylinder ($j \; j > a$) such that the inverse remains single-valued. If $j \; j = a$, the positive imaginary solution of Equation (3) is chosen.

In order to preserve the shape of the cylinder, a set of image vortices are introduced inside the cylinder in accordance with the Circle Theorem [17]. The complex potential in this case can be finally written as:

$$w(\ ) = U_1[\ + \frac{c_0^2}{\ }] + \frac{i\ _0}{2\ ^3}\sum_{n=1}^{\infty}[\ln(\ \ _0) + \ln(\ \ _n)\ \ \ln(\ \ _0 + \frac{c_0^2}{\ ^{1\!/\!4}_n\ \ _0})] \tag{4}$$

where $_0$ is the center of the cylinder, and $^{1\!/\!4}$ is the conjugate of . The real part of the above function is the velocity potential . The flow velocity on the body surface can be determined as the gradient of this function on the body surface.

$$U(z) = [\ \ (\frac{@}{@x})^2 + (\frac{@}{@y})^2]_{z=z_0} \tag{5}$$

The pressure $P(z)$ on the body surface can be computed using Bernoulli's equation

$$[\frac{P(z)}{\ } + \frac{1}{2}U^2(z) + \frac{@}{@t}]_{z=z_0} = C \tag{6}$$

where C is an absolute constant.

2.2 Model of the flow inside the canal

In this study, the canal is modeled as a long-slight tube with pores distributed along the surface of the tube at certain intervals. The diameter of this tube is taken to be 250um, and diameter of each pore is 250um as well, while the interval between two adjacent pores is taken to be 4mm. Because viscous e ect of the fluid inside canal cannot be neglected while the Reynolds Number of this flow is much smaller than 1, the momentum equation is then simplified to a linear equation. Hence, superposition is applicable in this case, the flow in the tube can considered respectively in each sub-segment

The flow inside canal is driven by pressure gradient between adjacent pores. Previous computational result indicates that the value of pressure along the vertical direction inside the LLTC at the pore location is essentially the external pressure at the opening [15]. Therefore, the pressure on the body surface where the canal opening is located dominates the flow inside canal.

If the vortex street passing the body has a infinite length, it can be predicted that the pressure at each opening will change periodically. Accordingly, the pressure gradient between adjacent pores can be written in Fourier series. Hence, the case of cosinoidal pressure di erence is considered.

$$P_L \quad P_R = jP_L \quad P_Rj\cos\ !t \tag{7}$$

where P_L and P_R are the pressures at left and right end of the tube, respectively. $jP_L \quad P_Rj$ and $!$ are the wave amplitude and angular frequency, respectively.

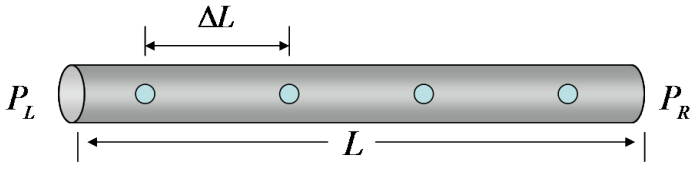

Figure 3: Schematic drawing of canal modeling

Flow driven by a periodic pressure gradient inside a tube of diameter D and length L has been solved analytically [18]. While the kinetic Reynolds number $!\frac{L}{D} = !(D=2)^2=\ ^1$, where ^{1} is the kinematic viscosity of the fluid inside the tube, is very small, which is valid for the case of LLTC, the induced velocity in the tube is in phase with the pressure oscillation. Flow velocity u_c of the fluid inside the tube, written in cylindrical coordinates, is given by

$$u_c = \frac{K}{4\ ^1}[(D=2)^2 \quad r^2]\cos\ !t = \frac{1}{4^{1\!/\!4}L}[(D=2)^2 \quad r^2)](P_L \quad P_R); \tag{8}$$

$$K = jP_L \quad P_R j=^2 L \tag{9}$$

where ^{2} and $¼$ are the density and dynamic viscosity of fluid inside canal, respectively. Therefore, the amplitude of velocity inside canal is proportional to the pressure gradient between two adjacent pores, and the change of velocity is in phase with the pressure oscillation.

2.3 Nondimensionalization

As shown in Figure 4, the computational domain is a fish-like body placed streamwise in a free stream flow with velocity U_1. The chord length of the fish-like body is c. A Karman vortex street is placed along one side of the body with horizontal and vertical distance between vortices l and b, respectively, and vortex strength . The location of the vortex street with respect to the body's frame of reference is discribed by the vertical distance between the center lines of fish body and vortex street.

For a stable Karman vortex street, the ratio of vertical distance between vortices, b, over horizontal distance, l, is kept to be 0.28 in present studies. According to potential flow theory, a Karman vortex street in static fluid moves itself in a velocity U_{tr} which is a function of the vortex street properties given by

$$U_{tr} = \frac{}{2l}\cot \frac{^3}{l}(l=2 + bi) \tag{10}$$

The velocity of vortex convecting downstream U_s is then taken to be the sum of U_1 and U_{tr}. Therefore, the nondimensionalization of independent variables governing the external flow field result in a set of three non-dimensional numbers $(\frac{l}{c}; \frac{h}{c}; \frac{}{cU_1})$.

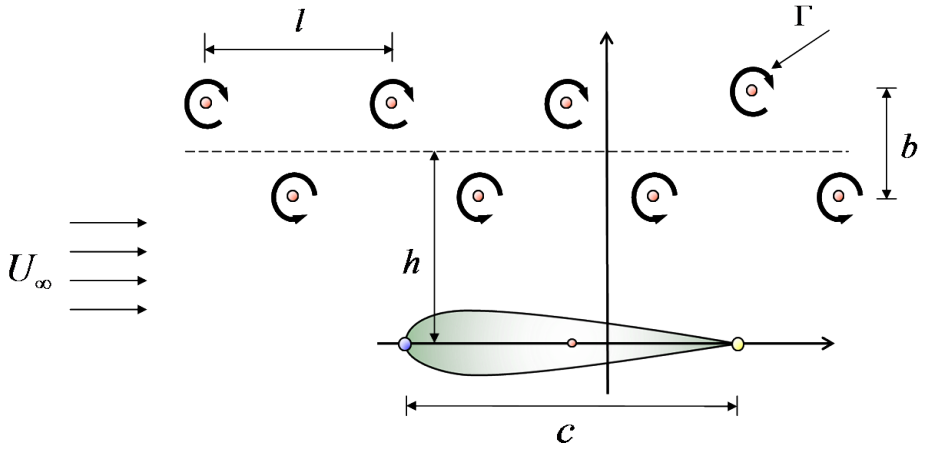

Figure 4: Schematic drawing of parameters governing the flow field.

3 Results & Discussion

3.1 Pressure created by single vortex

The case that a single fish body in free stream without presence of vertices is first studied. A single vortex is then placed close to the body. The pressure coe cients, defined by $C_p = P=\frac{1}{2}{}^2U_1$,of the two cases are showed in Figure 6. The pressure distribution along the body surface cearted by free stream without vortex is a single curve, with one low peak near the front. A single vortex placed close to the body will change the flow field and thus e ect the pressure on the body surface. The presence of a single vortex is indicated by a peak in the pressure curve. The location corresponds to the horizontal location of the vortex with respect to the body.

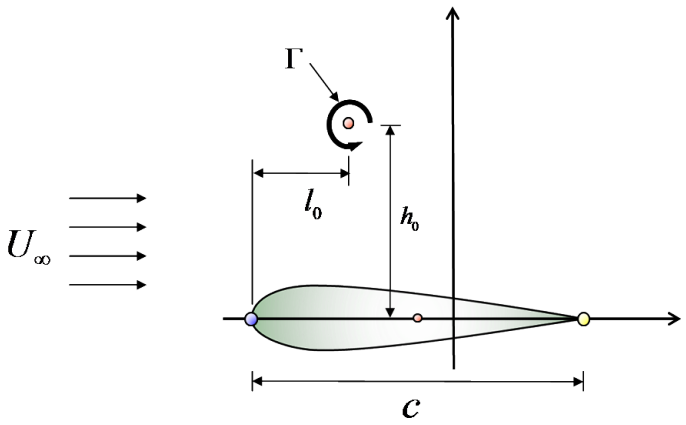

Figure 5: Schematic showing parameters of a single vortex close to a fish-like body.

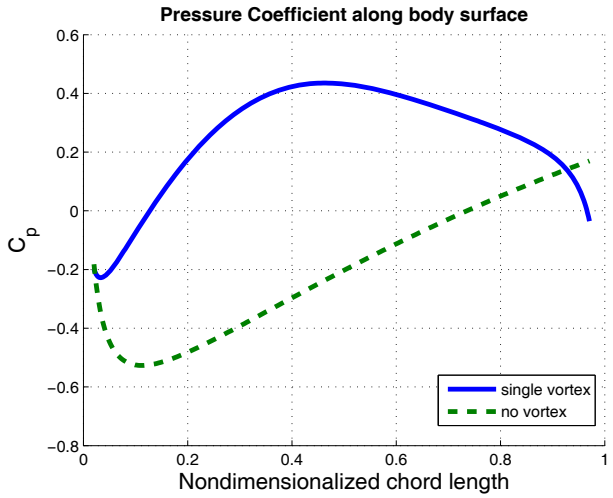

Figure 6: Pressure distribution along body surface with and without single vortex. Parameters are taken as $l_0 = 0.4c$, $h_0 = 0.6c$ and $\quad = 1$.

The e ects of changing circulation of vortex, , and distance between body and the vortex, h_0, have been studied. As shown in Figure ??, changing of the two parameters will neither add extra features to the pressure curve nor change the location of the peak, however, amplitude of the peak changes. The amplitude of the peak increases as the strength of the vortex increases or the distance decreases. Therefore, the information of a single vortex can be detected by measurement of the peak in pressure distribution along the body surface.

3.2 Sensing of convecting vortex street

As a vortex street is placed close to the body, the pressure distribution on the body surface is modified in a manner that is similar to the case of single vortex discussed above. The pressure distribution is shown in Figure 9, in which the number of vortices along the projection area of the body is identical to the number of peaks. As the vortex street passes the body, the pressure distribution on body surface changes with time and the locations of those peaks move downstream. If the length of vortex street is infinite, the change of pressure is periodical. Figure 10 shows the oscillation of pressure on three consecutive pores located at 0.5 unit of body length. The pressure changes are found to be in a wave mode close to a cosinoidal wave with the same periodicity as the Karman street, while the amplitudes and phases of those waves are di erent.

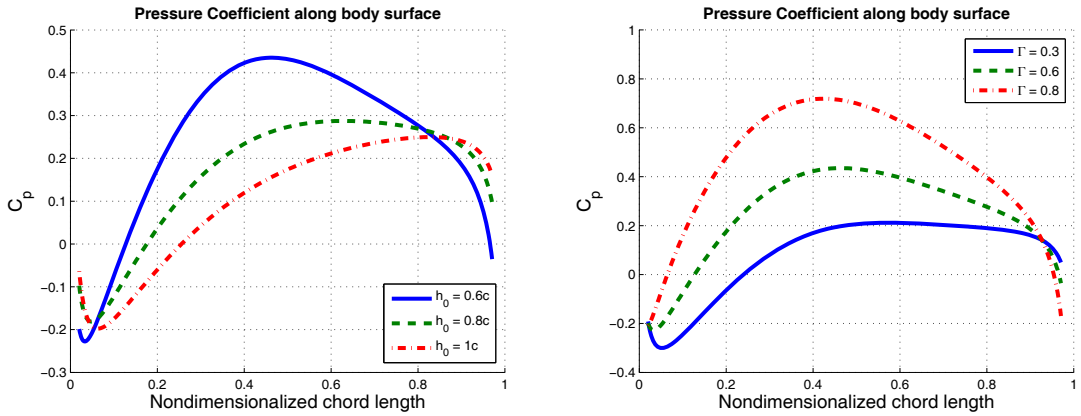

(a) Changing of distanc, h_0, between vortex and body

(b) Changing of vortex strength,

Figure 7: Pressure distribution along the body surface changes with variations of parameters.

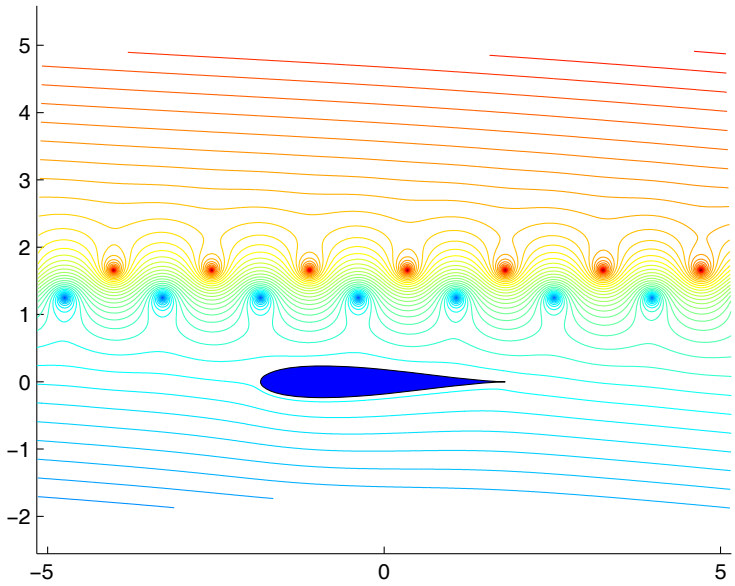

Figure 8: Stream lines of computational domain of a vortex street convecting along one side of a fish-like body. Parameters are taken as l=0.4c and h=0.4c.

Because the pressure on the body surface changes in a wave mode, the pressure gradient between consecutive pores also changes in wave mode with time, as shown in Figure 11. With the pressure gradient at consecutive pores known, the flow velocity inside LLTC is simply in phase with the pressure oscillation, and the amplitude is proportional to the pressure gradient, as discussed in previous chapter. The spacing of adjacent pores is assume to be infinite small in this section for convenience. Hence, the flow velocity distribution inside canal is successive. The validation of this assumption will be discussed in the next section.

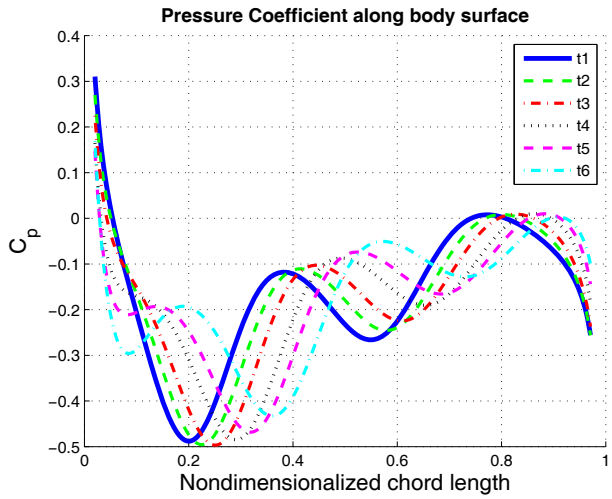

Figure 9: Pressure along the body surface changing with time. Time steps from t1 to t6 are taken from one quater of a cycle, with one vortex aligned to the leading edge of the body at time t1. Parameters are taken as l=0.4c and h=0.4c.

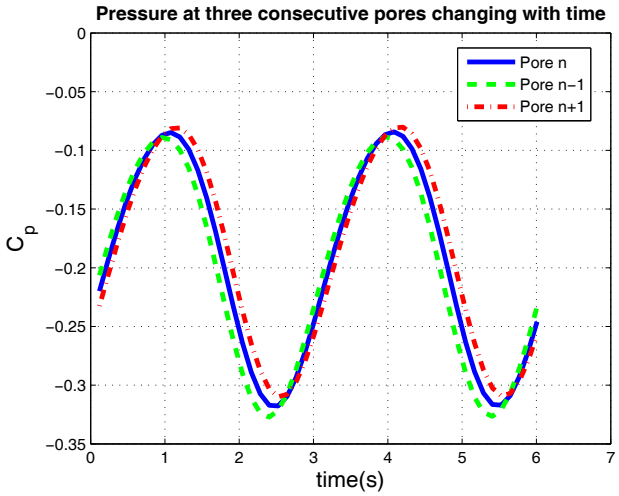

Figure 10: Pressure at three consecutive pores changing with time. Pores are located at 0.5c. Parameters are taken as l=0.4c and h=0.4c.

The flow velocity distibution inside the canal is shown in Figure 12. It can be observed that the number of peaks corresponds to the number of vortex pairs along the projection area of fish body, while the locations of those peaks correspond to the locations of vortex pairs. This observation can be verified in Figure 13, and stands in all cases studied. As horizontal distance between vortices changes, the distance between velocity peaks inside the canal changes as well. Accordingly, The distance between vortices,l, can be approximately determined by measurement of velocity peaks in the LLTC.

Various combinations of h (vertical distance between body and vortex street) and l (horizontal distance between vortices) have been investigated. The case of vortex street far from the body is shown in Figure 14. In this case, signature of the vortices can not be evidently seen from the distribution of flow velocity , while the existing of such vortices can still be detected by sensing the oscillation of flow velocity in the LLTC.

The case of vortex street close to the body is shown in Figure 15. In addition to major peaks indicating

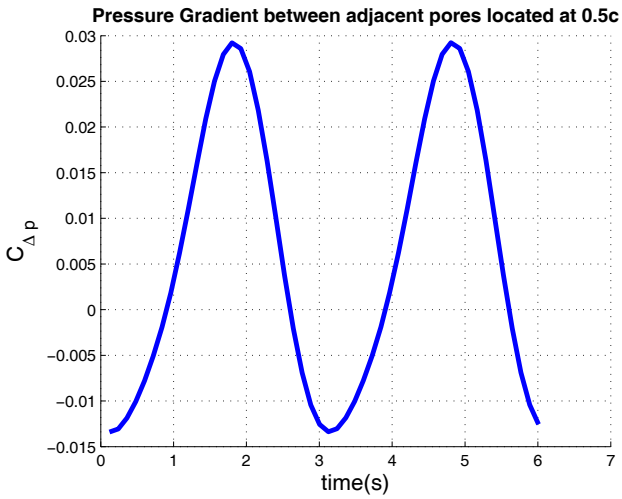

Figure 11: Oscillation of Pressure gradient between two adjacent pores located at 0.5c. Parameters are taken as l=0.4c and h=0.4c.

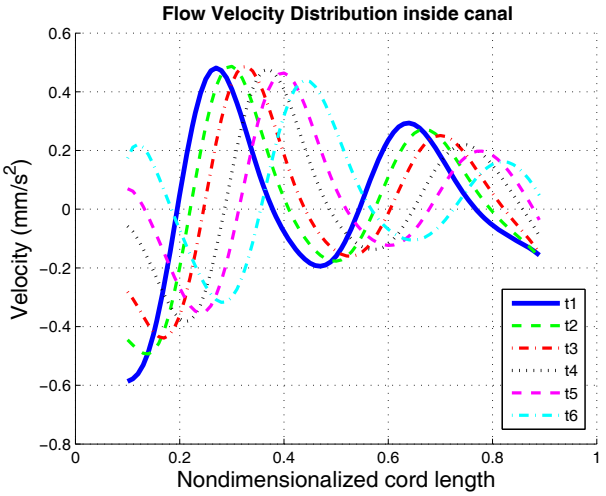

Figure 12: Flow velocity distribution in the canal. Parameters are taken as l=0.4c and h=0.4c.

vortex pairs in pressure distribution curve, a secondary peak can be found next to it, which is due to opposite vortices on the far side of the vortex street from the body. The secondary peaks can also be seen in the flow velocity distribution and velocity oscillation curves. As the vortex street comes even closer to the body, the secondary peak grows as well, which suggests that distance between the body and vortices may be estimated by measurement of the secondary peak.

3.3 Sensing resolution

Since the flow velocity in each sub-segment of the LLTC is determined by the pressure gradient between its two ends, the length of the sub-segment is of importance in sensing of a certain pressure field. Any pressure changes in a distance smaller than the length of the sub-segment, namely the spacing of pores, may not be detected by the LLTC. In this sense, the dimensions of the LLTC determine the sensing resolution of such system. In oder to detect a certain vortex street, the spacing of pores of a LLTC should be much smaller than

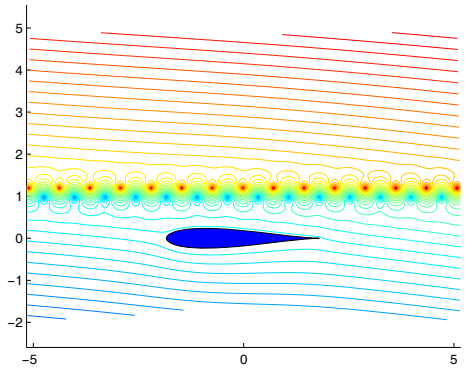

(a) Drawing of stream lines in computational domain

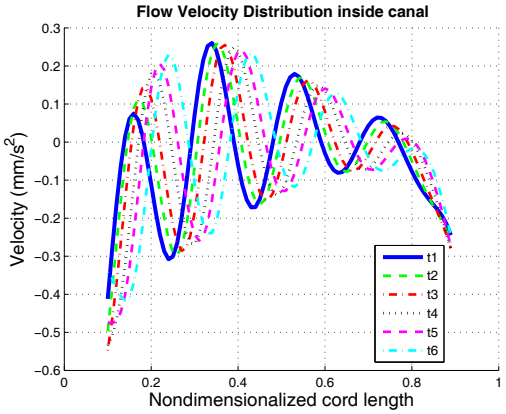

(b) Flow velocity distribution inside canal

Figure 13: Case of small distance between vortices. Parameters are taken as l=0.2c and h=0.3c. The number of peaks in the plot corresponds to the number of vortex pairs along the projection area of the body.

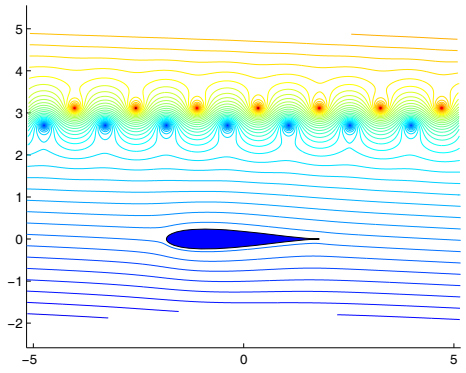

(a) Drawing of stream lines in computational domain

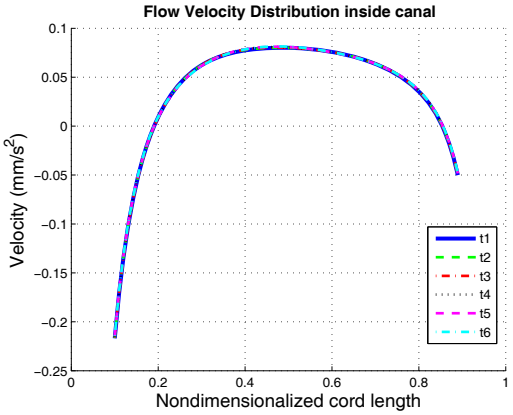

(b) Flow velocity distribution inside canal

Figure 14: Case of vortices far from body surface. Parameters are taken as l=0.4c and h=0.8c. The signature of vortex street is not evident.

the characteristic length of the vortex street. On the other hand, the length of the LLTC also determines how much information of the vortex street can be obtained. It is evident that longer LLTC would be helpful to collect more information of the flow field around.

In the previous section, the resolution of the LLTC is assumed to be infinite, which means the flow velocity inside LLTC is proportional to external pressure gradient. With consideration of pore spacing ÐL, several cases have been studied. The flow velocity inside LLTC for di erent ÐL value is showed in Figure 16. The typical pore spacing of LLTC of fish is around the order of 0.01 unit of body length. The pressure gradient recorded by such canal has fairly good accuracy as to infinite sensing resolution. As pore spacing increase, the resolution is poor and details of surrounding flow field can be lost. If the streamwise period of

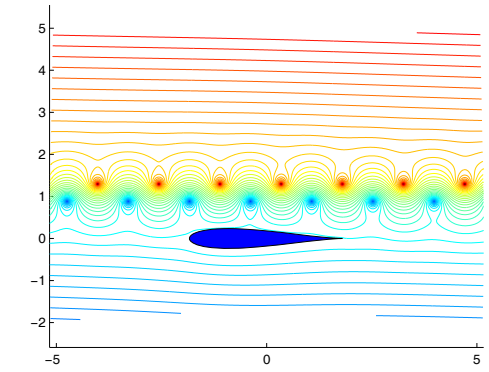

(a) Drawing of stream lines in computational domain

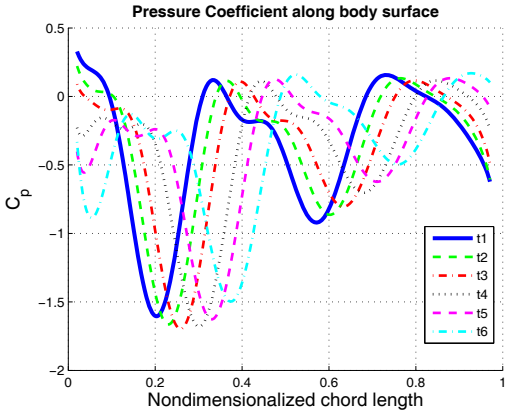

(b) Pressure distribution along body surface

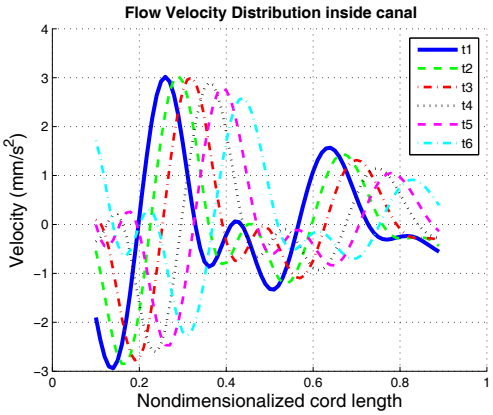

(c) Flow velocity distribution inside canal

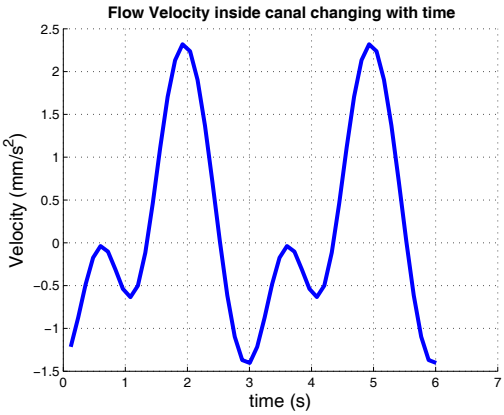

(d) Oscillation of flow velocity in sub-segment located at 0.5c

Figure 15: Case of vortices close to body surface. Parameters are taken as l=0.4c and h=0.3c. Secondary peak can be observed in the last two plots.

the Karman street is less than pore spacing, $l < Ð L$, fish is not able to detect the vortex street. This result may account for generally small pore spacings found in di erent fishes.

4 Conclusions

A two-dimensional, inviscid, irrotational flow model about a fish-like body with vortices close to it was developed, and pressure distribution on the body surface has been computed according to the model. With the external flow known, the lateral line trunk canal of a fish is modeled. The flow inside canal driven by the pressure gradient between a pair of consecutive pores can be solved analytically.

In order to determine the e ect of various flow parameters, parametric studies are performed. The results indicate changes of governing parameters also result in changes of flow velocity distribution inside the LLTC. The distance between vortices, can be approximately determined by measurement of velocity peaks in the LLTC, while distance between the body and vortices may be estimated by measurement of the secondary

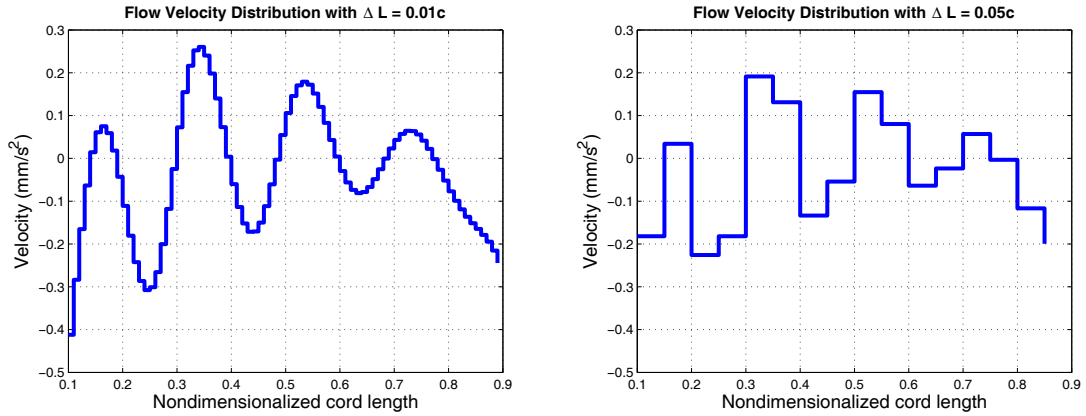

(a) Ð L = 0:01c (b) Ð L = 0:05c

Figure 16: Flow velocity inside canals with di erent pore spacings

peak. Previous studies suggest that the canal neuromast found in the LLTC of a fish is able to detect the local flow velocity inside the canal, which means fish is able to measure the distribution of flow velocity over the canal. Therefore, it is reasonable to suggest that the LLTC of a fish is able to detect not only the presence of a wake but also the signature of the wake.

Because the potential flow theory and Joukowski transformation were used to develop the model for this investigation, the constructure of the flow field with a fish-like body is of great flexibility. Further studies in this area could be conduct for vortex based detection such as obstacle detection and fish schooling.

Acknowledgements

Acknowledge support from ONR.

References

[1] H. Münz, "Single unit activity in the peripheral lateral line system of the cichlid fish", Sarotherodon niloticus L. J. Comp. Physiol. A 157, 555-568, 1985

[2] G.G. Harris, W.A. van Bergeijk, "Evidence that the lateral line organ responds to near field displacements of sound sources in water", J Acoust Soc Am 34:1831–1841, 1962

[3] H. Bleckmann, "Reaction time and stimulus frequency in prey localization in the surface-feeding fish Aplocheilus lineatus", J Comp Physiol A 140:163–172, 1980

[4] H. Bleckmann, "Role of the lateral line in fish behaviour". In: Pitcher TJ (ed) Behaviour of Teleost fishes", 2nd edn. Chapman & Hall, London pp 201–246, 1993

[5] B.L. Partridge, T.J. Pitcher, "The sensory basis of fish schools: relative roles of lateral line and vision", J Comp Phys 135:315–325, 1980

[6] E.S. Hassan, "On the discrimination of spatial intervals by the blind cave fish (Anoptichthys jordani)", J Comp Physiol A 159:701–710, 1986

[7] A.B.A. Kroese, N.A.M. Schellart, "Velocity- and acceleration-sensitive units in the trunk lateral line of the canal", J. Neurophysiol. 68, 2212–2221, 1992

[8] S. van Netten, "Hydrodynamic detection by cupulae in a lateral line canal:functional relations between physics and physiology", Biol Cybern 94: 67šC85, 200

[9] S. Coombs, M. Hastings and J. Finneran, "Modeling and measuring lateral line excitation patterns to changing dipole source locations", J. Comp. Physiol. A 178, 359-371, 1996

[10] A.B.A. Kroese, J.M. Van der Zalm and J. Van den Bercken "Frequency response of the lateral-line organ of Xenopus laevis", Pflügers Arch. 375, 167-175, 1978

[11] R.A. Handelsman, J.B. Keller, "Axially symmetric potential flow around a slender body", J Fluid Mech 28:131-147,1967

[12] E.S. Hassan, "Mathematical description of the stimuli to the lateral line system of fish derived from a three-dimensional flow field analysis. I. The cases of moving in open water and of gliding towards a plane surface", Biol. Cybern. 66, 443-452, 1992

[13] E.S. Hassan, "Mathematical description of the stimuli to the lateral line system of fish derived from a three-dimensional flow field analysis. II. The case of gliding alongside or above a plane surface", Biol. Cybern. 66, 453-461, 1992

[14] E.S. Hassan, "Mathematical description of the stimuli to the lateral line system of fish, derived from a three-dimensional flow field analysis. III. The case of an oscillating sphere near the fish", Biol. Cybern. 69, 525-538, 1993

[15] C. Barbier, "Drag force acting on a neuromast in the fish lateral line trunk canal. I. Numerical modeling of external-internal flow coupling", J.R.Soc. Interface. 6, 627-640, 2008

[16] I. Cohen and P. Kundu, "Fluid Mechanics", Academic Press, New York, 2007.

[17] L.M. Milne-Thomson, "Theoretical Aerodynamics", Dover, New York, 1958.

[18] F.M. White, "Viscous fluid flow", New York, NY: McGraw-Hill, Inc. 1974